PROTEINS
STRUCTURE ■ FUNCTION ■ BIOINFORMATICS

Structures of paraoxon-inhibited human acetylcholinesterase reveal perturbations of the acyl loop and the dimer interface

Matthew C. Franklin, Michael J. Rudolph, Christopher Ginter, Michael S. Cassidy, and Jonah Cheung*

Special Projects Group, New York Structural Biology Center, New York, New York 10027

ABSTRACT

Irreversible inhibition of the essential nervous system enzyme acetylcholinesterase by organophosphate nerve agents and pesticides may quickly lead to death. Oxime reactivators currently used as antidotes are generally less effective against pesticide exposure than nerve agent exposure, and pesticide exposure constitutes the majority of cases of organophosphate poisoning in the world. The current lack of published structural data specific to human acetylcholinesterase organophosphate-inhibited and oxime-bound states hinders development of effective medical treatments. We have solved structures of human acetylcholinesterase in different states in complex with the organophosphate insecticide, paraoxon, and oximes. Reaction with paraoxon results in a highly perturbed acyl loop that causes a narrowing of the gorge in the peripheral site that may impede entry of reactivators. This appears characteristic of acetylcholinesterase inhibition by organophosphate insecticides but not nerve agents. Additional changes seen at the dimer interface are novel and provide further examples of the disruptive effect of paraoxon. Ternary structures of paraoxon-inhibited human acetylcholinesterase in complex with the oximes HI6 and 2-PAM reveals relatively poor positioning for reactivation. This study provides a structural foundation for improved reactivator design for the treatment of organophosphate intoxication.

Proteins 2016; 84:1246–1256.

Key words: acetylcholinesterase; acyl pocket loop; crystal structure; paraoxon; organophosphate; insecticide; oxime; nerve agent.

INTRODUCTION

Acetylcholinesterase (AChE) is an essential enzyme that terminates neurotransmission by hydrolyzing the neurotransmitter acetylcholine in the synapse.[1] The catalytic site contains the catalytic triad (Ser, His, Glu) and lies at the base of a 20 Å deep active site gorge.[2] The peripheral site of the gorge contains aromatic side chains that aid substrate trafficking through the gorge.[3] Organophosphate (OP) compounds such as Schedule 1 chemical warfare nerve agents and insecticides irreversibly inhibit the enzyme. They react with S203 in the catalytic site to form a covalent phosphoester conjugate, leading to death through paralysis from inhibition of AChE in tissues involved in respiratory control. Enzymatic activity can be restored by administration of oxime reactivators that function as nucleophiles to chemically remove the conjugate from the catalytic serine.[4] A limitation of oximes is that they are not universally effective against all OPs.[5] Furthermore, over time the inhibited enzyme may age and become completely resistant to

Additional Supporting Information may be found in the online version of this article.

Matthew C. Franklin's current address is Regeneron Pharmaceuticals, Tarrytown, New York, New York, 10591.

Abbreviations: AChE, acetylcholinesterase; DMSO, dimethyl sulfoxide; hAChE, human acetylcholinesterase; HI6, 1-(2-hydroxy-iminomethylpyridinium)-1-(4-carboxyamino)-pyridinium dimethylether dichloride; OP, organophosphate; RMSD, root-mean-square deviation; 2-PAM, 2-pyridine aldoxime.

The atomic coordinates and structure factors for POX-hAChE, POX^{aged}-hAChE, POX*-hAChE, POX-hAChE:HI6, and POX-hAChE:2-PAM have been deposited into the Protein Data Bank under codes 5HF5, 5HF6, 5HF8, 5HF9, and 5HFA, respectively.

Institution at which work was performed: New York Structural Biology Center

Jonah Cheung and Matthew C. Franklin contributed equally to this work

MCF and JC designed the experiments. MCF, MJR, MC, CG, and JC performed the experiments. JC wrote the manuscript

*Correspondence to: Jonah Cheung, New York Structural Biology Center, New York, NY 10027. E-mail: jcheung@nysbc.org

Received 6 January 2016; Revised 18 April 2016; Accepted 8 May 2016

Published online 18 May 2016 in Wiley Online Library (wileyonlinelibrary.com).

DOI: 10.1002/prot.25073

reactivation through dealkylation of the conjugate.[6] There is no known antidote to reactivate aged OP-inhibited hAChE.

Although nerve agent attacks are sensationalistic, more people are routinely poisoned by OP pesticides than by nerve agents. Due to their widespread use in agriculture in the developing world, it is estimated that there are up to 3 million cases of death and acute poisoning due to pesticide exposure each year.[7] The current standard treatment for pesticide poisoning involves administration of atropine and oximes even though the effectiveness of oxime therapy is contested by physicians.[8] The physicochemical properties and pharmacokinetics may differ between OP pesticides and nerve agents, thus complicating treatment.[9]

The typical OP is a phosphate ester that contains a leaving group and two alkyl chains that remain attached to the phosphorous atom after conjugation with the catalytic serine. A distinguishing feature of many OP pesticides is that the two alkyl chains are identical, typically methoxy, ethoxy, and isopropoxy groups. The resulting phosphate formed after inhibition by pesticides is achiral. In contrast, traditional OP nerve agents are chiral as they contain two different alkyl chains, where one is a methyl group in the case of VX, VR, sarin, soman, and cyclosarin. The insecticide paraoxon (*O,O*-diethyl *O*-(4-nitrophenyl) phosphate) is an OP insecticide containing two ethoxy chains. The oxon form is more toxic and is derived from the less potent thion form (parathion (*O,O*-diethyl *O*-(4-nitro-phenyl) phosphorothioate)) by liver metabolism.[10] In contrast, nerve agents do not require bioactivation for extreme toxicity.

In this study, we present crystal structures of human AChE (hAChE) inhibited by paraoxon in unaged and aged states, and in unaged ternary complexes with oxime reactivators 1-(2-hydroxy-iminomethylpyridinium)-1-(4-carboxyamino)-pyridinium dimethylether dichloride (HI6) and 2-pyridine aldoxime (2-PAM). We observe significant conformational changes to the acyl loop within the active site gorge that provide structural insights into the disparities of oxime effectiveness in treating OP pesticide and nerve agent poisoning. We also see additional novel changes at the dimer interface due to inhibition. These results may guide new treatment strategies.

MATERIALS AND METHODS

Expression, purification, and crystallization of hAChE

A stable mammalian cell line expressing recombinant hAChE[11] was adapted to serum-free growth media by repeated serial passage of adherent cells in T75 tissue culture flasks (Corning) with media containing varying mixtures of increasing amounts of FreeStyle 293 Expression Medium (Gibco) and decreasing amounts of adherent growth media (DMEM GlutaMAX (ThermoFisher Scientific) supplemented with 10% fetal bovine serum (FBS) (Gibco)). After serum-free adaptation, the cells were transferred into sterile square media bottles for suspension growth in serum-free media to high densities for protein production.[12] Secreted hAChE was purified directly from serum-free media after clearing by centrifugation and filtration through a 0.22 μm filter (Pall Corporation), and finally crystallized in the ligand-free state following previously described methods.[11]

Formation of hAChE complexes

Binary complexes were formed by soaking hAChE crystals in 30 μL aliquots of crystallization buffer containing 1 m*M* paraoxon (Chem Service Incorporated), in nine-well glass plates (Hampton Research) sealed with clear tape. Crystals were cryostabilized and flash frozen in liquid nitrogen according to established protocols[11] after soaking durations ranging from 3 h to 7 days. All soaks were performed at 22°C, except when to promote aging, crystals were soaked at 30°C for 7 days in a temperature-controlled incubator. To form ternary complexes, an initial 3-h paraoxon soak was followed by a soak in cryostabilization solutions containing either HI6 or 2-PAM at 5 m*M* (10 min. soak) and 50 m*M* (30 min. soak), respectively, prior to freezing.

Data collection, structure determination, and analysis

Synchrotron X-ray data were collected at beamlines X25 and X29 of the National Synchrotron Light Source (NSLS) at Brookhaven National Laboratory. Integration and scaling was performed using HKL2000[13] and structure factors were calculated using CCP4.[14] The ligand-free hAChE structure [Protein Data Bank (PDB) code 4EY4] and the same free-R test set was used as a starting point for refinement using Refmac.[15] As required, conformationally variable regions of acyl loops, organophosphate adducts, and oxime reactivators were manually built into positive difference electron density using Coot[16] and refined using Refmac and Phenix.[17] Occupancy groups were created for atoms of OP adducts and oximes and refined, and restrained individual isotropic B-factors of all atoms were refined with automatic optimization of weights. For crossvalidation, 5% of reflections excluded from refinement of the same R-free column was used across all data sets. RAPIDO[18] was used to identify rigid protein backbone regions using a 0.5 Å lower cutoff limit, LSQMAN[19] was used to perform structural superimpositions by least squares alignment of C^{α} atoms, and PyMOL (Schrödinger) was used to create molecular graphics. Data collection and refinement statistics are listed in Table I.

Table I
Data Collection and Refinement Statistics

Data collection	POX-hAChE	POX^{aged}-hAChE	POX*-hAChE	POX-hAChE:HI6	POX-hAChE:2-PAM
Beamline	NSLS X29	NSLS X29	NSLS X25	NSLS X29	NSLS X29
d_{min} (Å)	2.15	2.3	2.8	2.2	2.2
wavelength (Å)	1.075	1.075	1.075	1.075	1.075
No. of observations	533,464	952,487	1,016,991	844,881	1,058,729
Multiplicity[a]	4.7 (4.1)	10.1 (6.2)	19.3 (19.9)	7.8 (6.4)	10.0 (5.3)
Average $(I)/(\sigma_I)$[a]	12.4 (1.1)	14.7 (0.9)	18.8 (3.6)	12.8 (0.3)	13.8 (0.8)
Completeness[a] (%)	99.7 (96.3)	99.9 (97.9)	100.0 (99.6)	99.5 (98.7)	99.3 (89.0)
R_{merge}[a,b] (%)	0.092 (0.891)	0.125 (1.412)	0.161 (0.922)	0.139 (3.165)	0.149 (1.305)
$CC_{1/2}$[a]	0.997 (0.600)	0.998 (0.627)	0.997 (0.931)	0.995 (0.661)	0.998 (0.685)
CC^{*}[a,c]	0.999 (0.866)	1.000 (0.878)	0.999 (0.982)	0.999 (0.892)	0.999 (0.902)
Refinement					
Bragg spacings (Å)	49.9–2.15	47.5–2.3	49.9–2.8	45.4–2.2	47.1–2.2
Space group	$P3_121$	$P3_121$	$P3_121$	$P3_121$	$P3_121$
Cell parameters: *a*, *b*, *c* (Å)	104.92, 104.92, 322.80	105.90, 105.90, 323.08	104.86, 104.86, 326.31	105.93, 105.93, 324.41	104.80, 104.80, 323.46
R^d/R^e_{free} (%)	17.4/20.6	17.4/20.6	15.6/20.0	20.1/24.0	18.1/22.4
No. of unique reflections	112,345	94,268	52,554	108,095	104,757
No. of total atoms (non-H)	9,256	9,023	8,738	9,133	9,173
No. of protein atoms (non-H)	8,399	8,367	8,370	8,350	8,421
No. of hetero atoms (non-H)	151	118	138	193	156
No. of waters	706	538	230	590	596
Average B-factor (Å^2)	42.3	54.7	48.4	48.2	47.3
rmsd bond length (Å)	0.011	0.009	0.007	0.010	0.010
RMSD bond angle (°)	1.23	1.20	1.03	1.21	1.21
Ramachandran favored/allowed[f] (%)	96.1/3.7	96.8/2.9	96.0/3.8	96.4/3.5	96.4/3.3
Z_a	2	2	2	2	2
PDB code	5HF5	5HF6	5HF8	5HF9	5HFA

[a]Values in outermost shell are given in parentheses.
[b]$R_{merge} = (\sum|I_i - <I_i>|)/\sum|I_i|$, where I_i is the integrated intensity of a given reflection.
[c]$CC^* = (2CC_{1/2}/1+ CC_{1/2})^{1/2}$.[40]
[d]$R = \sum||F_o| - |F_c||/\sum||F_o||$, where F_o and F_c denote observe and calculated structure factors, respectively.
[e]R_{free} was calculated using 5% of data excluded from refinement.
[f]Calculated using Molprobity.[41]

Measurements of aging in paraoxon-inhibited hAChE

Paraoxon at 20 m*M*, dissolved in 100% dimethyl sulfoxide (DMSO), was added to hAChE (25 μ*M*) in 0.1 *M* sodium phosphate (pH 7.4) buffer to a concentration of 1 m*M*. DMSO was added to a separate solution of enzyme to 5% (v/v) final concentration as a negative control, and both were incubated at 22°C. Aliquots were removed at various times post-inhibition and passed twice through 0.5 mL Zeba Spin 40 kDa molecular weight cutoff desalting columns, pre-equilibrated with sodium phosphate buffer, to remove paraoxon, reaction products, and DMSO. Enzyme concentrations were measured in triplicate by UV spectrophotometry and then diluted to 10 μM in phosphate buffer. HI6 from a 40 m*M* aqueous stock was added to 1 m*M* to the paraoxon-inhibited and paraoxon-free samples which then were incubated at 37°C for 30 min. Paraoxon-inhibited positive control samples were generated by adding water in place of HI6. Samples were subsequently diluted 1000-fold prior to activity determination using the QuantiChrom Acetylcholine Assay Kit (BioAssay Systems) and a 96-well plate reader (Beckman Coulter DTX 880). The percentage of unnaged hAChE remaining at each sampling was determined from the fraction of activity between paraoxon-inhibited samples and corresponding paraoxon-free negative controls, after reactivation. A sample processed immediately after paraoxon inhibition ($t = 0$) showed >98% recoverable activity after reactivation with HI6 (data not shown). Positive controls displayed less than 2.5% of the activity of the negative control, and there was no significant reduction of hAChE activity level over time in negative control. Reactivation measurements were performed in triplicate and calculated mean values are reported.

RESULTS AND DISCUSSION

Overview of reaction scheme, reactivators, and structures

Paraoxon inhibition of hAChE [Fig. 1(A)] results in covalent attachment of a diethylphosphate ester to the side-chain of the catalytic serine. The conjugate ages over time through spontaneous dealkylation of the adduct, forming a negatively charged monoethylphosphate that resists reactivation by oximes such as HI6 and 2-PAM [Fig. 1(B,C)]. In this study, we present structures of binary complexes of hAChE inhibited by paraoxon in

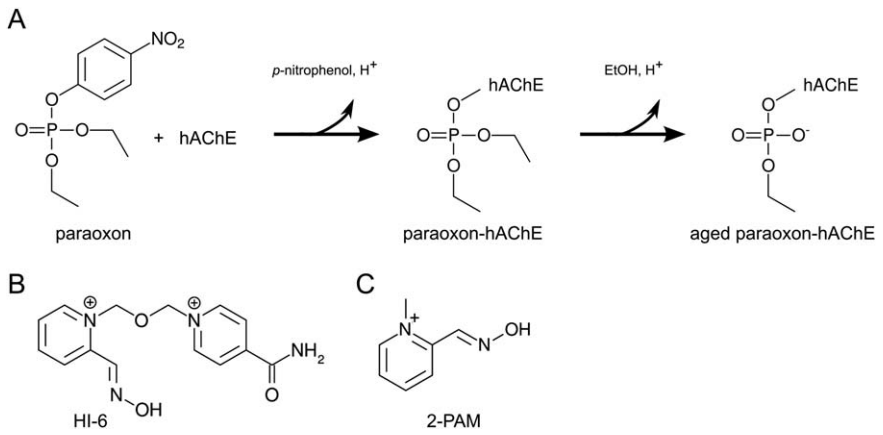

Figure 1

Chemical reaction and structures relevant to this study. (**A**) Inhibition of hAChE by paraoxon and subsequent aging of the complex. (**B**) Chemical structure of HI6. (**C**) Chemical structure of 2-PAM.

different states: POX-hAChE, paraoxon-inhibited hAChE in the unaged state; POX*-hAChE, paraoxon-inhibited hAChE in a partially aged state; and POX^{aged}-hAChE, paraoxon-inhibited hAChE in an aged state. We also present structures of ternary complexes of unaged paraoxon-inhibited hAChE bound to oximes HI6 and 2-PAM (POX-hAChE:HI6, POX-hAChE:2-PAM, respectively). All structures are isomorphous with ligand-free hAChE[11] and each subunit contains an accessible active site gorge. Data collection and refinement statistics are listed in Table I.

Binary complexes POX-hAChE, POX^{aged}-hAChE, and POX*-hAChE show a perturbed acyl loop

Significant positive electron difference density consistent with phosphorylation of S203 is seen after paraoxon soaking. In POX-hAChE, electron density features clearly define a diethylphosphate adduct [Fig. 2(A)] consistent with an unaged state, formed after a 24 hour soak. A longer soak for 7 days at 30°C results in positive difference density features consistent with an aged monoethylphosphate in POX^{aged}-hAChE [Supporting Information Fig. S1(A)].[20–22] Except for differences in the phosphate adducts, the structures of POX-hAChE and POX^{aged}-hAChE are similar, and our analysis focuses on POX-hAChE as the resolution is higher. Difference density consistent with an intermediate state of aging is seen in POX*-hAChE, formed from a 4 day soak [Fig. 2(B)]. The extent of aging seen in these structures is consistent with *in vitro* measurements (Supporting Information Fig. S2).

The binary complex structures of POX-hAChE and POX^{aged}-hAChE

In the unaged POX-hAChE structure [Fig. 3(A)], atomic B-factors of the ethoxy groups in the adduct refine to similar values compared to nearby atoms in the active site. One ethoxy faces the cationic site [W86; not drawn in Fig. 3(A)] and the other faces the acyl pocket (F295, F297, and F338). The phosphonyl oxygen is coordinated within hydrogen bonding distance to the amide nitrogens of G121 (2.9 Å), G122 (2.7 Å), and A204 (3.1 Å; not drawn in Fig. 3) of the oxyanion hole. This is consistent with the coordination of OPs seen in other AChE structures.[20,21] In POX-hAChE, atoms of the H447 side-chain are shifted by up to 0.7 Å relative to that in the ligand-free state, placing Nϵ2 of H447 within hydrogen bonding distance to both Ser203 Oγ (3.2 Å) and the phosphate O2 (3.1 Å). Hydrogen bonding within the catalytic triad remains intact (H477 Nδ1 to E334 Oϵ1 distance 2.8 Å) and the catalytic histidine side-chain does not appear to be as mobile as seen in VX-inhibited *Torpedo californica* AChE[23] and tabun-inhibited mouse AChE.[24] In POX^{aged}-hAChE (Supporting Information Fig. S2), there is a minor 0.5 Å shift in the relative position of the phosphate compared to POX-hAChE. The elimination of the ethoxy group that faces the cationic site through aging reduces the size of the adduct and creates a negative charge that forms electrostatic interactions with the H477 side-chain, resulting in altered position within the catalytic site. Hydrogen bonding appears unaffected as the adduct is stabilized in a similar manner as in POX-hAChE.

Extensive structural perturbations in residue positions 280–297, a region that encompasses most of the acyl loop (positions 287–299), are seen in both POX-hAChE and POX^{aged}-hAChE. Both structures have an acyl loop conformation similar to each other but different from the apo state. Superimposition of corresponding acyl loop Cα atoms with the ligand-free state[11] yields a root-mean-square deviation (RMSD) of 1.3 Å. Compared to the ligand-free state, phenyl ring atoms of F295 are shifted by an average distance of 3.3 Å, through a combination of side-chain rotation and a 2.7 Å Cα displacement. Main chain displacements are also seen in Y337 (∼0.5 Å) and F338 (∼1 Å). The greatest change occurs

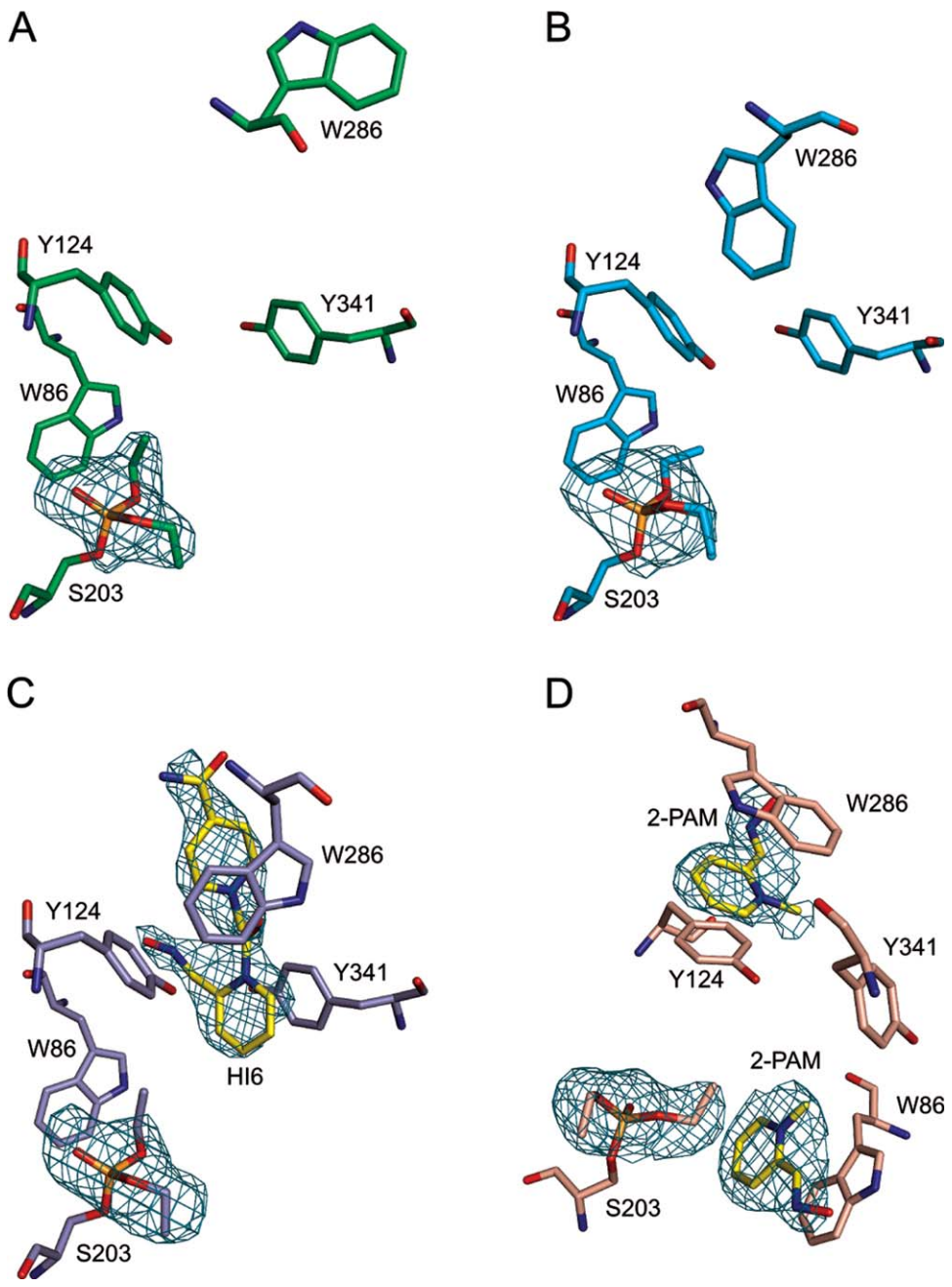

Figure 2

Simulated annealing omit electron density maps. (**A** and **B**) Positive electron difference density corresponding to phosphate adducts in POX-hAChE and POX*-hAChE, respectively. (**C** and **D**) Electron density for phosphate adducts and oximes in POX-hAChE:HI6 and POX-hAChE:2-PAM, respectively. The teal mesh represents the $|F_o| - |F_c|$ electron density omit map contoured at 3.0σ. Active site gorge residues, adducts, and reactivators, are drawn as sticks. In (B) only the higher occupancy monoethylphosphate adduct is drawn. Note that in (D), the orientation of the structure is rotated along the vertical axis by ~90° with respect to the others for greater clarity. Carbon atoms of the oximes are colored yellow, and carbon atoms of protein residues are colored by complex: POX-hAChE (green), POX*-hAChE (teal), POX-hAChE:HI6 (light blue), and POX-hAChE:2-PAM (salmon). Nitrogen, oxygen, and phosphorus atoms are colored dark blue, red, and orange, respectively.

with the highly mobile R296 where the Cα and the side-chain shift by 4.9 Å and 14.9 Å (measured from Cζ positions), respectively. The side-chain is displaced from a position hydrogen bonded to the side chains of H405 and N406 in the ligand-free state, where it extends away from the gorge, to a position within the peripheral site stabilized by π-stacking of the guanidinium group against the hydroxyphenyl ring of Y72. It displaces the indole ring of W286, and accommodating rotations point the side chains of W286 and H287 away from the gorge

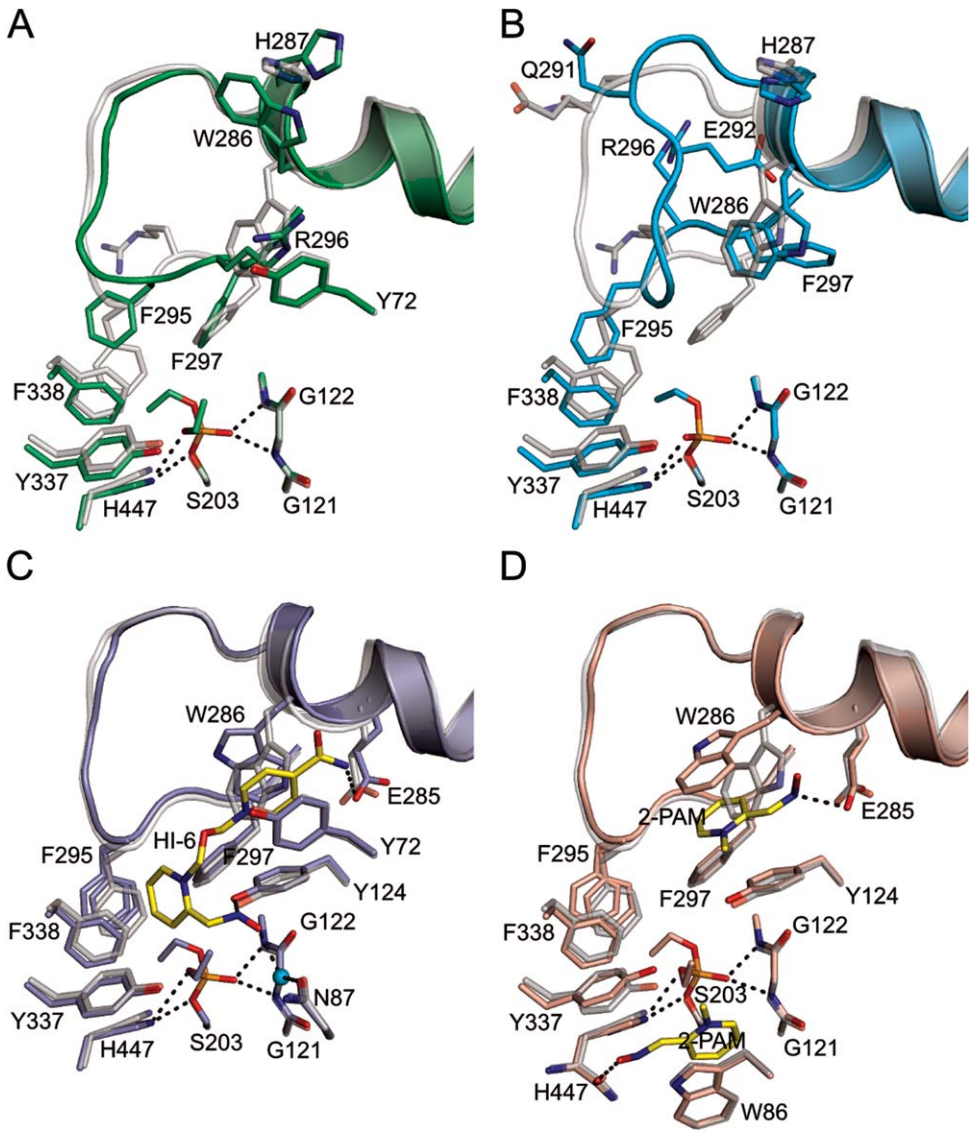

Figure 3

Conformational changes induced by paraoxon inhibition. (**A–D**) Structural perturbations seen in POX-hAChE, POX*-hAChE, POX-hAChE:HI6, and POX-hAChE:2-PAM are visualized by superimposition with ligand-free hAChE. The coloring scheme of Figure 2 is used. Carbon atoms of ligand-free hAChE are colored semi-transparent gray. Residues of the helix preceding the acyl loop and of the acyl loop up to position 298 are drawn as ribbons. Atoms of select residues, reactivators, and phosphate adducts are drawn as sticks. Water is drawn as a teal sphere and hydrogen bonds are depicted by dashed gray lines.

toward the bulk solvent. Higher B-factors and less well defined electron density around the side chains of R296, W286, and H287 indicate more disorder.

The binary complex structure of POX*-hAChE

Unexpectedly, a different acyl loop conformation is seen in a set of three crystals soaked with paraoxon for 4 days, and POX*-hAChE is solved from the best crystal of this set. The features of positive difference density at the location of the phosphate [Fig. 2(B)] suggests partial aging, and a mixture of mono- and diethylphosphates conjugated to S203 is modeled and refined to fractional occupancies of 0.8 and 0.2, respectively. The acyl loop conformation in POX*-hAChE differs from both ligand-free hAChE and POX-hAChE, and superimposition of corresponding acyl loop Cα atoms with each yields RMSD values of 1.9 Å and 2.4 Å, respectively. In POX*-hAChE, a substantial backbone rearrangement between Residues 289 and 296 reorients the side chains of Q291 and E292. Atoms of the F295 phenyl ring are shifted on average by 2.3 Å, and the Cα is displaced by 2.0 Å, with respect to ligand-free hAChE. The side-chain of F297

adopts a different rotomer and the Cα is shifted by 1.3 Å. Changes in R296 are less dramatic than in POX-hAChE but still significant; the Cα is shifted by 2 Å and the side-chain adopts a different rotomer, extending away from the peripheral site to a position stabilized through electrostatic interaction with the side-chain of E243, located 4 Å away. Patches of residual difference density appearing in the final cycles of refinement suggested a possible low occupancy fraction of another acyl loop conformation; however, the quality of the density does not allow for accurate modeling.

It is unlikely that the acyl loop conformation seen in POX*-hAChE is related to aging of the adduct as we see no interactions of the eliminated ethyl chain with the acyl loop. As the phosphate-facing side chains of the acyl loop are uncharged, an electrostatic mechanism for adopting that conformation is also unlikely. Other soaking experiments timed to form states of partial aging resulted in the formation of the acyl loop conformation seen in POX-hAChE. The conformational heterogeneity due to paraoxon inhibition may be related to other unexpected perturbations in the lattice discussed later.

Significant acyl loop perturbations seen in binary complexes of hAChE with paraoxon appear to stem from interactions between the F295 phenyl ring and the ethoxy group of the adduct positioned in the acyl pocket. Due to the relatively crowded local environment, a side-chain rotation of F295 is insufficient to accommodate the adduct, and instead shifts in residue backbone positions are necessary to avert steric clash. Large acyl loop backbone rearrangements have also been seen in mouse AChE and *T. californica* AChE inhibited by the OP pesticide diisopropyl fluorophosphate (DFP),[20,22] but not in the hAChE:fasciculin-II complex inhibited by tabun in the aged state,[25] the only other reported structure of OP-inhibited hAChE solved to date. A more recent structure of DFP-inhibited mouse AChE (PDB code 5HCU)[26] shows significantly less perturbation of the acyl loop; however, high atomic B-factors of the adduct suggest improper modeling of full occupancies in a complex that is likely only partially formed. Differences in acyl loop conformations seen in hAChE and mouse AChE when inhibited by paraoxon and DFP likely results from differences in the van der Waals volumes of the formed adducts. Acyl loop perturbations are not seen in an aged complex of *T. californica* AChE inhibited by methyl paraoxon (PDB code 3GEL) in which a methoxy group is placed in the acyl pocket, but AChE complexes formed from insecticides containing methoxy groups such as malathion or methylchlorpyrifos are also poorly reactivated by oximes.[27]

Structural perturbation of active site gorge residues by OP inhibition, which may block oxime accessibility to the adduct, has been proposed as a mechanism for inefficient reactivation.[28] In both POX-hAChE and POX*-hAChE, a narrowing of the gorge in the peripheral site occurring with the perturbed acyl loop, and placement of the R296 side-chain in the peripheral site of POX-hAChE, could present a steric barrier to the entry of oximes or affect oxime binding; however, potential electrostatic effects of the side-chain on entry of positively charged pyridinium oximes are likely not significant due to the large dipole moment of AChE.[29] These results suggest that there may be a structural component to the generally inefficient oxime reactivation of AChE when inhibited by OP pesticides rather than by nerve agents.[27] Stereoselective inhibition of AChE by OP nerve agents that place a methyl group into the acyl pocket do not affect the acyl loop in the same manner.[23,24]

Binding of HI6 and 2-PAM in paraoxon-inhibited hAChE

In POX-hAChE:HI6, the features of observed positive difference density [Fig. 2(C)] are consistent with phosphorylated S203 and bound HI6 [Fig. 3(C)]. The adduct is coordinated in the same manner as previously described, but refines to a lower occupancy of 0.80 as reactivation occurs in the crystal during soaking with HI6. We focus on describing the complex in chain B as the occupancy of bound HI6 is higher and corresponding positive difference density is of better quality. The carboxyamino-pyridinium ring of HI6 is sandwiched between the side chains of W286 and Y72 in the peripheral site by π-stacking interactions; the indole ring of W286 rotates from the ligand-free conformation to allow for this interaction. In this position, the carboxyamino nitrogen of HI6 lies within hydrogen bonding distance to the side-chain of E285 (3.1 Å). Unlike in other AChE complexes containing bound HI6 where the carboxyamino-pyridinium ring is seen π-stacked between the aromatic side chains of W286 and Y124,[30–32] this pose of HI6 more closely resembles that of bound HLö-7 in the B monomer of a ternary complex of mouse AChE inhibited by tabun.[28] Toward the catalytic site, the oxime-pyridinum ring of HI6 is stabilized by π-stacking to the side-chain of Y341, and by van der Waals contacts with the side chains of Y337, F338, and Y124. A direct hydrogen bond is formed between the nitrogen atom of the oxime group and the side-chain oxygen of Y124 (2.9 Å), and a water-mediated hydrogen bond is formed with the side-chain oxygen of N87. In chain A, HI6 is bound with a different orientation of the oxime-pyridinum ring stabilized by hydrogen bonding between the oxime oxygen and the backbone nitrogen of F295 (3.0 Å). This is similar to HI6 bound in mouse AChE.[33] The binding of HI6 in POX-hAChE:HI6 does not appear to be ideal for reactivation. In both chains A and B, the oxime group points away from the adduct and is separated by 9.0 Å and 9.7 Å from the phosphorous atom, respectively.

In POX-hAChE:2-PAM, positive difference density features are also consistent with phosphorylation of the

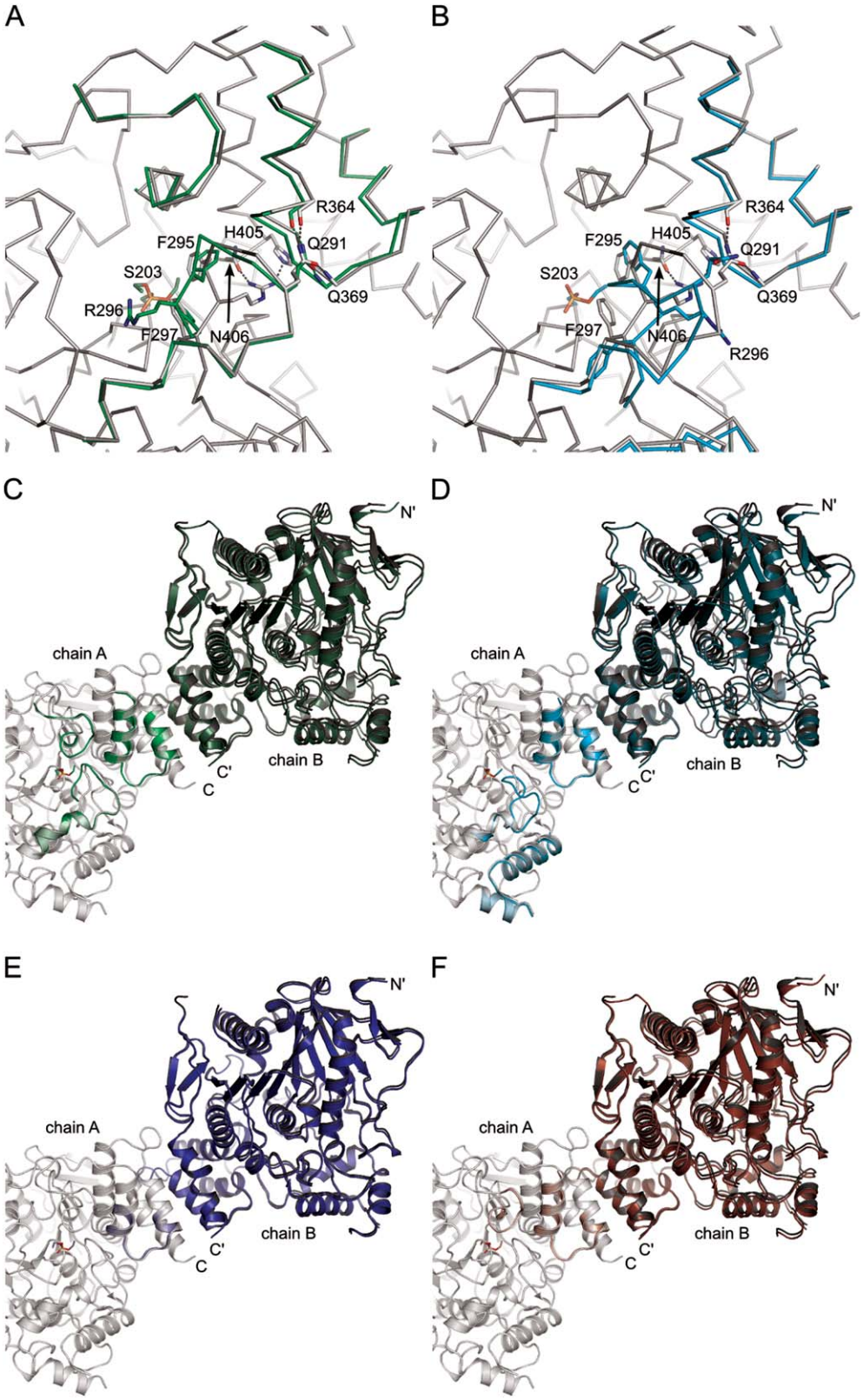

Figure 4

Perturbations of the hAChE dimer. (**A** and **B**) Chain A of POX-hAChE and POX*-hAChE, respectively, are superimposed with chain A of ligand-free hAChE (gray Cα trace) by alignment of conformationally invariant Cα positions. Only conformationally variable regions of the complexes are shown as Cα traces, following the same coloring scheme as Figure 2, with side chains and phosphate adducts drawn as sticks. This orientation provides a view into the active site gorge from a vantage point external from the peripheral site. (**C–F**) POX-hAChE, POX*-hAChE, POX-hAChE:HI6, and POX-hAChE:2-PAM, respectively, are superimposed with ligand-free hAChE (chains A aligned) to show perturbations of the dimer. Subunits of hAChE are drawn as ribbons and shown from a more distant vantage point, but in the same orientation as (A) and (B).

catalytic serine and a molecule of 2-PAM bound in each of the peripheral and catalytic sites [Fig. 2(D)]. The adduct is coordinated as previously seen and refines to an occupancy of 0.81. The peripheral site-bound 2-PAM is sandwiched by π-stacking between the side chains of W286 and Y124, and the side-chain of W286 adopts a different rotomer than in POX-hAChE:HI6 or the ligand-free state [Fig. 3(D)]. Additional interactions include van der Waals contacts with the side chains of Y72 and F297, and hydrogen bonding between the oxime nitrogen and the side-chain of E285 (2.9 Å). In the catalytic site, 2-PAM is bound by π-stacking with the side-chain of W86, and by hydrogen bonding of the oxime oxygen with the backbone oxygen of H447 (2.7 Å). The binding of 2-PAM in *T. californica* AChE and human butyrylcholinesterase inhibited by aged soman is similar.[21,34] In POX-hAChE:2-PAM, additional interactions include van der Waals contacts between 2-PAM and the ethoxy group (4 Å) that faces the cationic site. In the catalytic site, 2-PAM is bound with the oxime group pointing away from the phosphate, located 8.7 Å away, and does not appear to be in a productive orientation for reactivation. As AChE conjugates with VX and tabun also show an ethoxy group placed in the cationic site,[23,35] we may expect a similar mode of 2-PAM binding in hAChE complexes with these OP nerve agents.

In these ternary complexes, the backbone conformation of the acyl loop resembles that of the ligand-free state and appears to be stabilized by oxime binding. The binding of HI6 in mouse AChE inhibited by fenamiphos shows a similar reversion.[32] Acyl loop distortions have been shown to reduce binding affinity of reactivators,[31] and this may affect reactivation kinetics. Superimposition of corresponding Cα atoms in POX-hAChE:HI6 and POX-hAChE:2-PAM with the ligand-free state yields RMSD values of 0.31 Å and 0.28 Å, respectively. There are close van der Waals contacts between the F295 phenyl ring and the phosphate (3.2 Å), but the acyl loop appears to be energetically constrained by bound oxime. With the exception of the W286 side-chain, which rotates to bind oxime, the rotomer conformation of other side chains in the acyl loop are generally unchanged. Electron density for the F295 phenyl ring is less well defined and it has been modeled in two alternate conformations. These conformations are reflective of the mixed states resulting from paraoxon-inhibition and partial reactivation in the crystal lattice.

Perturbations of the dimer interface

Additional structural perturbations extending away from acyl loop are seen in the binary complexes when they are compared with ligand-free hAChE.[11] Using the RAPIDO server,[18] regions of backbone flexibility are identified in Residues 337–349 and 355–379 in POX-hAChE, and in Residues 240–273 and 356–379 in POX*-hAChE [Fig. 4(A,B)]. Cα atoms are displaced by up to 1.1 Å as atomic interactions with the acyl loop are altered. At the dimer interface, there are displacements of up to 0.8 Å in Cα positions in one of the helices, resulting in 1.2° and 2.1° rotations in the relative orientations of subunits in the biological dimer of POX-hAChE and POX*-hAChE, respectively [Fig. 4(C,D)]. This affects molecular packing in the lattice but does not significantly alter overall unit cell dimensions. It likely that these different states resulting from paraoxon inhibition are energetically similar, and may be influenced by lattice force effects.[36,37] These changes are less pronounced in the ternary complexes [Fig. 4(E,F)] in which subunits are rotated by less than 1° due to stabilization of a more apo-like conformation of the acyl loop with bound oxime. These perturbations of the hAChE dimer interface and crystal lattice are novel and are not seen in other complexes of hAChE bound to small molecules.[11,38] Conformational changes in other AChE homologs due to OP-conjugation and small molecule binding are limited to the active site gorge and do not show the same heterogeneity we see with paraoxon.[20,32,39]

CONCLUSION

This study elucidates the unique conformational changes that occur in hAChE upon inhibition by the OP insecticide paraoxon. These large structural perturbations, likely to be expected from inhibition by other OP pesticides, appear distinct from changes resulting from inhibition by traditional OP nerve agents, and stem from specific structural differences between pesticides and nerve agents. Owing to the placement of comparatively larger alkyl chains in the acyl pocket, a perturbed acyl loop due to hAChE inhibition by OP pesticides may impede reactivation. In addition to contributing to greater understanding of hAChE function, this work potentially aids development of more effective treatments for OP exposure which is critical due to their widespread use in the developing world.

ACKNOWLEDGMENTS

The authors thank Wayne A. Hendrickson and David Hirsh for their comments on the manuscript. We also thank the staff of beamlines X29 and X25 at the National Synchrotron Light Source for their assistance in data collection. Use of the National Synchrotron Light Source, Brookhaven National Laboratory is supported by the U.S. Department of Energy, Office of Science, Office of Basic Energy Sciences, under contract no. DE-AC02-98CH10886. This work was funded by New York Structural Biology Center.

REFERENCES

1. Taylor P, Radić Z. The cholinesterases: from genes to proteins. Annu Rev Pharmacol Toxicol 1994; 34:281–320.
2. Sussman JL, Harel M, Frolow F, Oefner C, Goldman A, Toker L, Silman I. Atomic structure of acetylcholinesterase from *Torpedo californica*: a prototypic acetylcholine-binding protein. Science 1991; 253:872–879.
3. Bourne Y, Taylor P, Radić Z, Marchot P. Structural insights into ligand interactions at the acetylcholinesterase peripheral anionic site. EMBO J 2003; 22:1–12.
4. Hobbiger F, Sadler PW. Protection by oximes of bis-pyridinium ions against lethal diisopropyl phosphonofluoridate poisoning. Nature 1958; 182:1672–1673.
5. Wilhelm CM, Snider TH, Babin MC, Jett DA, Platoff GEJ, Yeung DT. A comprehensive evaluation of the efficacy of leading oxime therapies in guinea pigs exposed to organophosphorus chemical warfare agents or pesticides. Toxicol Appl Pharmacol 2014; 281:254–265.
6. Shafferman A, Ordentlich A, Barak D, Stein D, Ariel N, Velan B. Aging of phosphylated human acetylcholinesterase: catalytic processes mediated by aromatic and polar residues of the active centre. Biochem J 1996; 318: 833–840.
7. Bertolote JM, Fleischmann A, Eddleston M, Gunnell D. Deaths from pesticide poisoning: a global response. Br J Psychiatry 2006; 189:201–203.
8. Eddleston M, Szinicz L, Eyer P, Buckley N. Oximes in acute organophosphorus pesticide poisoning: a systematic review of clinical trials. QJM 2002; 95:275–283.
9. Thiermann H, Szinicz L, Eyer P, Felgenhauer N, Zilker T, Worek F. Lessons to be learnt from organophosphorus pesticide poisoning for the treatment of nerve agent poisoning. Toxicology 2007; 233:145–154.
10. Chambers JE, Chambers HW, Snawder JE. Target site bioactivation of the neurotoxic organophosphorus insecticide parathion in partially hepatectomized rats. Life Sci 1991; 48:1023–1029.
11. Cheung J, Rudolph MJ, Burshteyn F, Cassidy MS, Gary EN, Love J, Franklin MC, Height JJ. Structures of human acetylcholinesterase in complex with pharmacologically important ligands. J Med Chem 2012; 55:10282–10286.
12. Muller N, Girard P, Hacker DL, Jordan M, Wurm FM. Orbital shaker technology for the cultivation of mammalian cells in suspension. Biotechnol Bioeng 2005; 89:400–406.
13. Otwinowski Z, Minor W. Processing of X-ray diffraction data collected in oscillation mode. Methods Enzymol 1997; 276:307–326.
14. Winn MD, Ballard CC, Cowtan KD, Dodson EJ, Emsley P, Evans PR, Keegan RM, Krissinel EB, Leslie AGW, McCoy A, McNicholas SJ, Murshudov GN, Pannu NS, Potterton EA, Powell HR, Read RJ, Vagin A, Wilson KS. Overview of the CCP4 suite and current developments. Acta Crystallogr D Biol Crystallogr 2011; 67:235–242.
15. Murshudov GN, Vagin AA, Dodson EJ. Refinement of macromolecular structures by the maximum-likelihood method. Acta Crystallogr D Biol Crystallogr 1997; 53:240–255.
16. Emsley P, Lohkamp B, Scott WG, Cowtan K. Features and development of Coot. Acta Crystallogr D Biol Crystallogr 2010; 66:486–501.
17. Adams PD, Afonine PV, Bunkóczi G, Chen VB, Davis IW, Echols N, Headd JJ, Hung L, Kapral GJ, Grosse-Kunstleve RW, McCoy AJ, Moriarty NW, Oeffner R, Read RJ, Richardson DC, Richardson JS, Terwilliger TC, Zwart PH. Phenix: a comprehensive python-based system for macromolecular structure solution. Acta Crystallogr D Biol Crystallogr 2010; 66:213–221.
18. Mosca R, Schneider TR. RAPIDO: a web server for the alignment of protein structures in the presence of conformational changes. Nucleic Acids Res 2008; 36:W42–6.
19. Kleywegt GJ. Use of non-crystallographic symmetry in protein structure refinement. Acta Crystallogr D Biol Crystallogr 1996; 52: 842–857.
20. Hörnberg A, Tunemalm A, Ekström F. Crystal structures of acetylcholinesterase in complex with organophosphorus compounds suggest that the acyl pocket modulates the aging reaction by precluding the formation of the trigonal bipyramidal transition state. Biochemistry 2007; 46:4815–4825.
21. Sanson B, Nachon F, Colletier J, Froment M, Toker L, Greenblatt HM, Sussman JL, Ashani Y, Masson P, Silman I, Weik M. Crystallographic snapshots of nonaged and aged conjugates of soman with acetylcholinesterase, and of a ternary complex of the aged conjugate with pralidoxime. J Med Chem 2009; 52:7593–7603.
22. Millard CB, Kryger G, Ordentlich A, Greenblatt HM, Harel M, Raves ML, Segall Y, Barak D, Shafferman A, Silman I, Sussman JL. Crystal structures of aged phosphonylated acetylcholinesterase: nerve agent reaction products at the atomic level. Biochemistry 1999; 38: 7032–7039.
23. Millard CB, Koellner G, Ordentlich A, Shafferman A, Silman I, Sussman JL. Reaction products of acetylcholinesterase and VX reaveal a mobile histidine in the catalytic triad. J Am Chem Soc 1999; 121:9883–9884.
24. Ekström F, Akfur C, Tunemalm A, Lundberg S. Structural changes of phenylalanine 338 and histidine 447 revealed by the crystal structures of tabun-inhibited murine acetylcholinesterase. Biochemistry 2006; 45:74–81.
25. Carletti E, Colletier J, Dupeux F, Trovaslet M, Masson P, Nachon F. Structural evidence that human acetylcholinesterase inhibited by tabun ages through O-dealkylation. J Med Chem 2010; 53:4002–4008.
26. Katz FS, Pecic S, Tran TH, Trakht I, Schneider L, Zhu Z, Ton-That L, Luzac M, Zlatanic V, Damera S, Macdonald J, Landry DW, Tong L, Stojanovic MN. Discovery of new classes of compounds that reactivate acetylcholinesterase inhibited by organophosphates. Chembiochem 2015; 16:2205–2215.
27. Musílek K, Kuca K, Jun D. Evaluation of potency of known oximes (pralidoxime, trimedoxime, HI-6, methoxime, obidoxime) to in vitro reactivate acetylcholinesterase inhibited by pesticides (chlorpyrifos and methylchlorpyrifos) and nerve agent (russian VX). Acta Med (Hradec Kralove) 2007; 50:203–206.
28. Ekström FJ, Astot C, Pang Y. Novel nerve-agent antidote design based on crystallographic and mass spectrometric analyses of tabun-conjugated acetylcholinesterase in complex with antidotes. Clin Pharmacol Ther 2007; 82:282–293.
29. Porschke D, Créminon C, Cousin X, Bon C, Sussman J, Silman I. Electrooptical measurements demonstrate a large permanent dipole moment associated with acetylcholinesterase. Biophys J 1996; 70: 1603–1608.
30. Artursson E, Andersson PO, Akfur C, Linusson A, Börjegren S, Ekström F. Catalytic-site conformational equilibrium in nerve-agent adducts of acetylcholinesterase: possible implications for the HI-6 antidote substrate specificity. Biochem Pharmacol 2013; 85:1389–1397.
31. Ekström F, Hörnberg A, Artursson E, Hammarström L, Schneider G, Pang Y. Structure of HI-6*sarin-acetylcholinesterase determined by X-ray crystallography and molecular dynamics simulation: reactivator mechanism and design. PLoS One 2009; 4:e5957
32. Hörnberg A, Artursson E, Wärme R, Pang Y, Ekström F. Crystal structures of oxime-bound fenamiphos-acetylcholinesterases: reactivation involving flipping of the His447 ring to form a reactive Glu334-His447-oxime triad. Biochem Pharmacol 2010; 79:507–515.
33. Ekström F, Pang Y, Boman M, Artursson E, Akfur C, Börjegren S. Crystal structures of acetylcholinesterase in complex with HI-6, ortho-7 and obidoxime: structural basis for differences in the ability to reactivate tabun conjugates. Biochem Pharmacol 2006; 72:597–607.
34. Wandhammer M, de Koning M, van Grol M, Loiodice M, Saurel L, Noort D, Goeldner M, Nachon F. A step toward the reactivation of aged cholinesterases–crystal structure of ligands binding to aged human butyrylcholinesterase. Chem Biol Interact 2013; 203:19–23.
35. Carletti E, Li H, Li B, Ekström F, Nicolet Y, Loiodice M, Gillon E, Froment MT, Lockridge O, Schopfer LM, Masson P, Nachon F.

Aging of cholinesterases phosphylated by tabun proceeds through O-dealkylation. J Am Chem Soc 2008; 130:16011–16020.
36. van Aalten DM, Crielaard W, Hellingwerf KJ, Joshua-Tor L. Conformational substates in different crystal forms of the photoactive yellow protein–correlation with theoretical and experimental flexibility. Protein Sci 2000; 9:64–72.
37. Rapp CS, Pollack RM. Crystal packing effects on protein loops. Proteins 2005; 60:103–109.
38. Cheung J, Gary EN, Shiomi K, Rosenberry TL. Structures of human acetylcholinesterase bound to dihydrotanshinone I and territrem B show peripheral site flexibility. ACS Med Chem Lett 2013; 4:1091–1096.
39. Rydberg EH, Brumshtein B, Greenblatt HM, Wong DM, Shaya D, Williams LD, Carlier PR, Pang Y, Silman I, Sussman JL. Complexes of alkylene-linked tacrine dimers with *Torpedo californica acetylcholinesterase*: binding of Bis5-tacrine produces a dramatic rearrangement in the active-site gorge. J Med Chem 2006; 49:5491–5500.
40. Karplus PA, Diederichs K. Linking crystallographic model and data quality. Science 2012; 336:1030–1033.
41. Chen VB, Arendall WBIII, Headd JJ, Keedy DA, Immormino RM, Kapral GJ, Murray LW, Richardson JS, Richardson DC. Molprobity: all-atom structure validation for macromolecular crystallography. Acta Crystallogr D Biol Crystallogr 2010; 66:12–21.